

The aero-acoustic resonance behavior of partially covered slender cavities

Arjen Teake de Jong · Hester Bijl ·
Fulvio Scarano

Received: 26 October 2010 / Revised: 19 June 2011 / Accepted: 23 June 2011 / Published online: 9 July 2011
© The Author(s) 2011. This article is published with open access at Springerlink.com

Abstract The present investigation focuses on the aero-acoustic resonance of cavities with a width much larger than their length or depth and partially covered, as often encountered in automotive door gaps. The cavities are under influence of a low Mach number flow with a relatively thick boundary layer. Under certain conditions, these cavities can acoustically resonate with the flow. The upstream and downstream edge of the opening as well as the cover lip overhang location and boundary layer thickness are parametrically varied in an experimental campaign, and the effect of the parameters on the resonance amplitude is investigated. Slender rectangular cavity geometries with an opening length of 8 mm and spanwise width of 500 mm are used. The cavity flow-induced acoustic response is measured with pressure transducers at different spanwise locations inside the cavity. Hot-wire measurements are performed to quantify the boundary layer characteristics. Furthermore, high-speed time-resolved particle image velocimetry is used to capture the instantaneous velocity field around the opening geometries. When the boundary layer thickness is increased, the cavity resonance amplitude diminishes. The cover lip overhang location has a large influence on the resonance response, which can be attributed to changes in the cavity driven flow properties. Rounding of the upstream edge promotes resonance, whereas rounding of the downstream edge can

diminish it. A possible explanation of the phenomenon is given on the basis of the PIV observations.

1 Introduction

The flow over cavities is often studied for their intrinsic resonant behavior and the consequent significance of aeroacoustic noise production (Rockwell and Naudascher 1979). Aero-acoustic research has focussed on a number of different cavity geometries, like for example cavities with cylindrical openings (Haigermoser et al. 2009). In the aircraft industry, most focus has been put on open shallow cavities. These cavities often resemble aircraft bays and landing gear wheel wells (Rossiter 1967). Deep cavity resonance has also been a topic of interest, for example in side branches of pipe systems (Radavich et al. 2001; Dequand et al. 2003). Generic partially covered cavity geometries have also been investigated in detail, where the cavity often behaves like a Helmholtz resonator. For example, Dequand et al. (2003, 2003) investigated the resonance lock-on amplitude of several rectangular Helmholtz resonator geometries under a thin boundary layer flow compared to the opening length. Examples of applications using partially covered cavities are the sound generation in flute-like instruments (Dequand et al. 2003; Coltman 1976; Elder 1973), the buffeting of open car sunroofs and side windows (Crouse et al. 2005; Ricot et al. 2001) and Helmholtz resonators used in acoustic liners (Ingard 1953).

The current investigation concerns the flow-induced resonance behavior of cavity configurations that are slender (width much larger than length or depth) and under influence of a flow with a thick boundary layer compared to opening length and partially covered. These configurations are relevant in the automotive industry because they

A. T. de Jong (✉) · H. Bijl · F. Scarano
Delft University of Technology, Kluyverweg 2,
2611 HS Delft, The Netherlands
e-mail: a.t.dejong@tudelft.nl

H. Bijl
e-mail: h.bijl@tudelft.nl

F. Scarano
e-mail: f.scarano@tudelft.nl

represent the properties of automobile door and trunk lid gaps. Under certain conditions, these gaps can resonate with the flow. Door gap like configurations with a high aspect ratio have not been examined in great detail. Nelson et al. (1981, 1983) experimentally analyzed a Helmholtz resonator with a slotted opening with an aspect ratio of 60 in the center of the resonator. Laser Doppler velocimetry was used, and the configuration was excited by a grazing flow of 17–26 m/s with a single boundary layer thickness. A detailed analysis of the flow was executed for this single configuration. In addition, Henderson (2000, 2004) presented benchmark experimental data of a resonator with an aspect ratio 55 opening and a thick and a thin boundary layer flow of 45–60 m/s. Only one single configuration was investigated, with a cover lip mounted from the upstream edge. A number of resonance modes were found; however, the physical mechanism for a number of these modes was not entirely clear. Mongeau et al. (1997) show experimental results of a varying aspect ratio around 30 that resembles a door gap, including a seal fixture. The cover lip was mounted on the upstream edge and the downstream edge was varied between a 90° sharp corner and a 45° one. The effect of the boundary layer thickness was not investigated and the flow speed was 16–43 m/s. The cavity only showed a passive linear response to the outside flow.

The effect of the boundary layer characteristics is known for cavities of non-slender open type. For open cavities, it is known that the boundary layer has a large influence on the resonance behavior (Ahuja and Mendoza 1995). For a non-slender resonator, Kooijman et al. (2008) showed that by increasing the boundary layer momentum thickness compared to the opening length, the instability of the opening shear layer is reduced. Howe's theory (1997) indicated that an increased aspect ratio modifies the impedance, thereby reducing the sensitivity to resonate due to a grazing flow. In fact, in general, automotive door gaps only show a passive response to the flow, although there are cases where a resonance lock-on can occur (Gloerfelt 2009). For the slender cavities and in particular with partial cover of the leading and trailing edge, the influence of the boundary layer properties on the resonance behavior is not sufficiently explored. In the present study, attention is focussed upon the effect of the boundary layer thickness to the onset of flow oscillations in the cavity.

For shallow open cavities and deep open cavities, like for example side-branches in pipe systems, the influence of the design of the upstream and downstream opening edges is considerable (Dequand et al. 2003; Kooijman et al. 2008; Rockwell and Knisely 1979; Gharib and Roshko 1987). The design of the opening edges is expected to have a large influence on gap resonance behavior as well, but this has not been investigated in detail to date. Mongeau showed that a modification of the trailing edge has an

influence on the response amplitude. Differences in resonance response between the various investigated geometries (Nelson et al. 1981, 1983; Henderson 2000, 2004; Mongeau et al. 1997) cannot be fully explained in terms of cavity dimensions and flow properties alone. Therefore, in the current investigation, three parameters concerning the cavity opening geometry are varied to investigate the effect of the opening design on the resonance properties. Both the upstream and downstream edges are varied. In addition, the cover lip overhang location is moved between the upstream and downstream edges in order to investigate the effect of the opening geometry in more detail.

The current investigation concerns door gap cavity resonance behavior in order to reveal the influence of upstream and downstream opening geometry, opening location with respect to the underlying cavity and relative boundary layer thickness on resonance. The study is conducted on a simplified geometry, where the parameters of interest are systematically varied. The opening edges are implemented with sharp or round edges, and the cover overhang location is moved between the upstream and downstream edges. PIV is known to be a valuable tool to assess the fluid mechanic behavior of cavities (Morris 2011). In order to quantify the effects of the parametric variations, high-speed PIV is adopted to measure the flow field velocity above and inside the cavity.

2 Cavity excitation and resonance theory

The fluid enclosed in the volume of a cavity can act as an acoustic resonator to an excitation source in the cavity neck region. Excitation can be either due to a feedback mechanism of the perturbed shear layer or due to passive excitation by the pressure fluctuations in the turbulent flow (turbulent rumble) (Elder et al. 1982). In case of feedback, the shear layer can roll up into discrete vortices impinging on the downstream edge coherently (a Rossiter mode) (Rossiter 1967), or exhibit a flapping shear layer motion. In the low Mach number limit, a feedback mode corresponds to excitation at a fixed Strouhal number $Sr = \frac{fL_o}{U_\infty}$, with f the resonance frequency, L_o the cavity streamwise opening length, and U_∞ the free stream velocity. If the excitation frequency is close to a resonance frequency, lock-on can occur and the system can resonate. In case of turbulent rumble, the resonance should effectively be independent of velocity (Elder et al. 1982).

The resonance mechanism can be either of a Helmholtz type or of a standing wave type. In Helmholtz-like resonance, the mass of air in the cavity is coherently compressed and expanded. The equation for a Helmholtz resonator is (Gloerfelt 2009):

$$f_H = \frac{c}{2\pi} \sqrt{\frac{S}{VH'_o}} \tag{1}$$

here, V is the cavity volume, S is the cavity neck surface area, and H'_o is the corrected vertical length of the cavity neck. The relation between the actual vertical cavity neck height H_o and H'_o is $H'_o = H_o + h$, where h is an end effect correction factor to account for the added resonating mass above and below the opening. For non-slender openings, it is based on the surface area $h \propto \sqrt{S}$, whereas in the slotted opening of the current investigation, it is assumed to be related to the opening length only $h \propto L_o$ and independent of the slot width W (Ingard 1953). For the currently investigated covered slender cavities, higher frequency resonance modes with spanwise variations can occur, where the mode frequency is dependent on the spanwise width (de Jong and Bijl 2010). The focus of the current investigation is the base Helmholtz mode.

For the currently investigated covered slender cavities, higher resonance modes with spanwise variations can be described by the following equation (de Jong and Bijl 2010):

$$f_n = \frac{c}{2\pi} \sqrt{\frac{S}{VH'_o} + \beta \left(\frac{\pi(n-1)}{W}\right)^2}, \tag{2}$$

with β of order 1, accounting for variations in resonator effective cross-section and widths. Note that this equation can be interpreted as the interaction between spanwise standing waves and Helmholtz resonance or as individual sections of the cavity acting as separate Helmholtz resonators that are coupled. The first $n = 1$ mode has constant properties along the span and corresponds to the Helmholtz mode. For the $n = 2$ mode, the opposite ends of the cavity are in anti-phase.

The normalized acoustic velocity amplitude $\frac{|d\epsilon/dt|}{U_\infty}$ in the neck region for a lumped mass system is a good indicator to evaluate the degree of acoustic lock-on (Dequand et al. 2003). It can be estimated by:

$$\frac{|d\epsilon/dt|}{U_\infty} \approx \frac{V_{cav}}{\rho_0 S} \frac{|dp|}{U_\infty} = \frac{1}{2} \sqrt{\frac{V_{cav}}{V_m}} \frac{|p'|}{q} M \tag{3}$$

with ϵ the acoustic displacement, $|p'|$ the amplitude of the cavity acoustic excitation, $q = \frac{1}{2}\rho U_\infty^2$ the dynamic pressure, M the Mach number, $V_{cav} = L_c H_c W$ the cavity volume, $V_m = L_o H'_o W$ the modified volume of the opening section. In the derivation, conservation of mass in the resonator is used. Also $dp = c^2 d\rho$ and Eq. 1 for the Helmholtz resonator are used.

To whether or not a cavity will have resonance a linear stability analysis of the shear layer over the opening can be employed. Using linear stability analysis, Michalke

(1965, 1969, 1970). derived the stability properties of shear layers with a tangent hyperbolic (tanh) profile. This theory is further used by Bruggeman et al. (1991) and Kooijman et al. (2008) for side branches in pipe flow. The tanh profile is stable for Strouhal numbers below $St_{\theta, \max} \equiv \frac{2\pi f \theta}{\Delta U} = 0.25$ (Kooijman et al. 2008).

In the next sections, Eq. 1 will be used to predict the resonance frequency of the investigated configurations and Eq. 3 will be used to observe if the resonance amplitude is of high or low amplitude (Dequand et al. 2003; Kooijman et al. 2008). Linear stability analysis of the tanh profile will be used to evaluate influence of the boundary layer properties on resonance and to evaluate the difference between shear layers of resonating and non-resonating geometries.

3 Experimental apparatus and procedure

3.1 Wind tunnel and model

Experiments are conducted in a low-speed open jet wind tunnel at Delft University of Technology. The tunnel has a vertical outflow through a circular opening, 0.6 m in diameter. The tunnel contraction ratio is 250:1. The airflow in the test section has a turbulence intensity of 0.2 and the wind tunnel acoustic background noise at 25 m/s is 20 dB.

The experimental geometry consists of a rectangular cavity partially covered by a rigid overhang plate attached at either the upstream or downstream corner of the cavity. The cavity opening is subjected to a flow with a thick (compared to the opening length L_o) boundary layer developed along a flat plate. Figure 1 shows the internal dimensions of the cavity. The aspect ratio of the cavity opening is $W/L_o = 62.5$, with a width of $W = 500$ mm. The base Helmholtz mode is expected to have coherent excitation along the span. The aspect ratio of the opening is chosen large enough $W/L_o \gg 1$ to ensure to be clearly in the slender regime. As Mongeau et al. (1997) indicated, the ratio of internal cavity length to the opening length can be

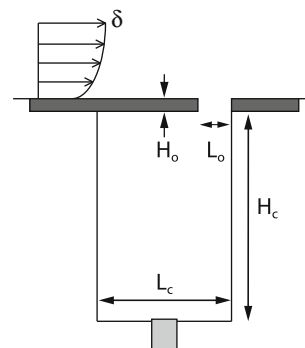


Fig. 1 Cross-sectional view of the cavity

of importance. Therefore, in the current investigation, the ratio of opening length and cavity internal length are set to resemble car door gaps more closely than similar configurations of Henderson (2000, 2004). The cross-sectional internal dimensions are $L_c \times H_c = 32 \times 50$ mm and the opening dimensions are $L_o \times H_o = 8 \times 3.2$ mm. The expected Helmholtz resonance frequency based on Eq. 1 is around 800 Hz and expected velocity of maximum resonance is 25 m/s.

The model used in the wind tunnel is a cavity embedded in a splitter plate which has an elliptic nose cone. Figure 2 shows the setup mounted in the wind tunnel nozzle. The boundary layer develops on the first section of the splitter plate, upstream of the cavity. The boundary layer is controlled in a precise and reproducible way by adjusting the length of the upstream section of the plate L_p . In the setup used for this publication, it is chosen as $L_p = [0.2, 0.3, 0.5, 0.7, 0.9]$ m. A zigzag type turbulator strip of 1 mm height is located 10 cm downstream of the leading edge to trigger the transition of the laminar boundary layer into a turbulent one. By changing the plate length, the expected boundary layer thickness is varied. The maximum spanwise width of the cavity is set to 0.5 m, which is smaller than the 0.6 m width of the splitter plate itself to ensure constant flow properties along the span.

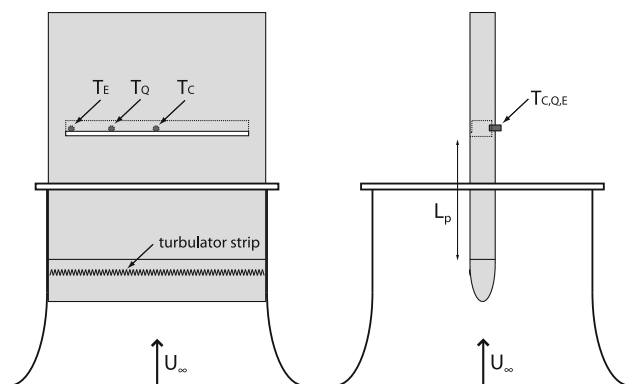


Fig. 2 Front and side views of splitter plate with cavity mounted in wind tunnel nozzle. Cavity internal pressure transducer T_C , T_Q , T_E locations indicated by arrows

The cavity itself is constructed out of thick-walled aluminum to ensure enough rigidity to prevent fluid-structure resonance effects. The cavity neck is equipped with sharp or round edges and an upstream or downstream cover lip overhang can be installed, leading to 8 different configurations investigated here. This is depicted in Fig. 3.

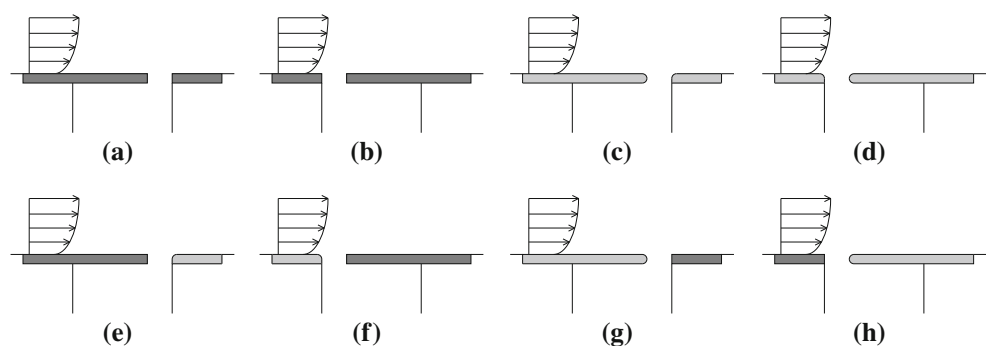
3.2 Measurement equipment

The boundary layer characteristics are measured with a constant temperature hot-wire probe in absence of a cavity, for 4 different flow speeds (20, 24, 30, and 40 m/s). Flow runs with open cavity have been performed to measure the flow-induced sound pressure levels inside the cavity. The velocity is increased incrementally, up to the wind tunnel limit of approximately 47 m/s. The cavity internal sound pressure level is recorded using 3 Druck Inc. PDCR 22 pressure transducers. These are located at different spanwise locations (center, quarter, and edge) on the floor of the cavity, as indicated in Fig. 1.

In order to evaluate the flow in the opening region, high-speed, time-resolved particle image velocimetry (PIV) has been used. The PIV measurements are also used to capture the lower boundary layer characteristics and will be combined with hot-wire results in Sect. 4. The PIV field of view is the region from 0 to 7 mm height in the boundary layer. Focus is put on the near wall region (0–0.5 mm) that is unresolved by hotwire measurements.

The illumination over an area of 25 by 16 mm is provided by a Quantronics Darwin-Duo 527 Nd:YLF laser. The field of view captures the cavity opening and the outer flow boundary layer up to 8 mm in height. The light sheet is positioned streamwise and perpendicular to the plate, with spanwise location 80 mm from the opening edge. A Photron Fastcam SA1.1 camera (1,024 × 1,024 pixels) is placed at a 90° angle with the illumination and captures 1,024 × 512 images. The illumination and recording devices are synchronized and controlled by a LaVision programmable timing unit (PTU v9) controlled by DaVis 7.3 software. Each measurement consists of 1,000 image pairs at a recording frequency of 6,000 Hz, which is

Fig. 3 Cavity opening configurations



sufficient to capture the temporal behavior of the flow (at approximately eight samples per resonance cycle). The double pulse interval is varied between 8 and 15 μs , depending on the velocity. The chosen magnification yields a typical digital resolution of 40 pixels/mm. The images were analyzed with the LaVision Davis 7.3 software, using a multi-step cross-correlation with a final interrogation window size of 16 by 16 pixels (0.4 by 0.4 mm^2) with 75% overlap.

4 Experimental results

The boundary layer properties as well as the cavity flow-induced response are presented in the current section. The cavity properties are evaluated for a single configuration (depicted in Fig. 3a). The boundary layer is evaluated using hot-wire and PIV. The cavity resonance behavior is evaluated using the internal pressure transducers, and the cavity opening flow field is evaluated using PIV results.

4.1 Incoming boundary layer

The boundary layer properties are obtained using both hot-wire and PIV measurements. Figure 4 illustrates the change in boundary layer mean flow characteristics due to variation in plate length L_p . PIV and hot-wire results are included in this figure. One can observe that the PIV results match the hot-wire results well.

Figure 5 shows a typical scaled logarithmic representation of the boundary layer properties, scaled by $u^+ = \frac{u}{v^*}$ and $y^+ = \frac{yv^*}{\nu}$, where v^* is the slip velocity and ν the kinematic viscosity (White 1991). There is a slightly higher wake component for the shortest ($L_c = 0.2$ m) plate. On overall, the shape of the boundary layer is a fully developed turbulent flat plate one, and the relative shape does not change with varying boundary layer thickness, indicating that self-similarity conditions are reached to a good degree.

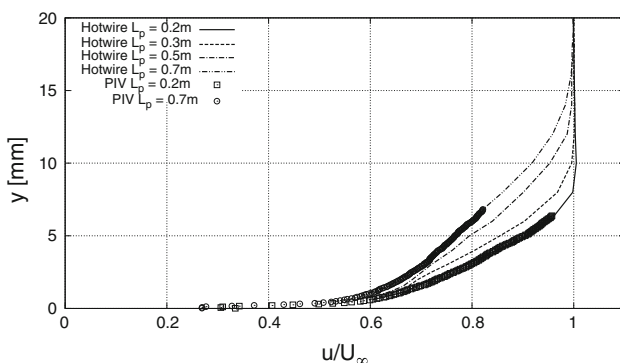


Fig. 4 Experimental boundary layer mean profiles for different plate lengths

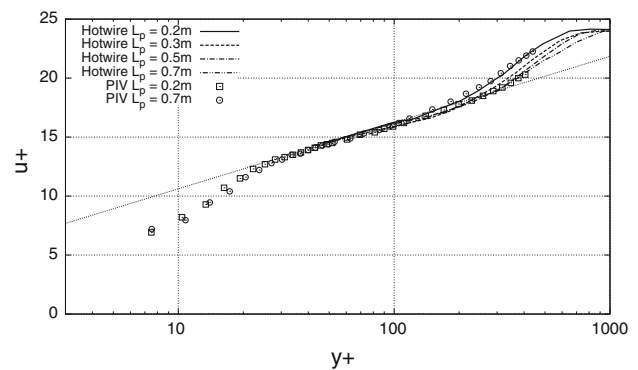


Fig. 5 Experimental boundary layer scaled logarithmic profiles for different plate lengths, scaled as $u^+ = \frac{u}{v^*}$ and $y^+ = \frac{yv^*}{\nu}$. A dashed line indicating the turbulent log layer region (White 1991) is added to the figure

The fact that the boundary layer shape is similar for all measured boundary layers can also be observed by evaluating the boundary layer integral properties given in Table 1. The following integral properties are evaluated; the displacement thickness δ^* , the momentum thickness θ , the shape factor H , and the height at 99% of the mean flow δ_{99} , as defined in (White 1991). The shape factor does not vary and corresponds to a value for a turbulent flat plate boundary layer (White 1991). Please note that in the table, the boundary layer properties for the 0.9 m plate are not measured, but estimated based on data for all smaller plate lengths. The shape factor is set as the average of the measured boundary layer shape factors. The other integral properties are extrapolated using a least-squares linear regression through the data.

4.2 Pressure fluctuations in the cavity

The cavity flow-induced resonance is investigated by measuring the internal pressure response. In the current section, the results for the upstream overhang with sharp edges (depicted in Fig. 3a) and $L_p = 0.7$ m are presented. This configuration shows typical resonance properties and resembles previously investigated geometries most closely (Henderson 2000, 2004).

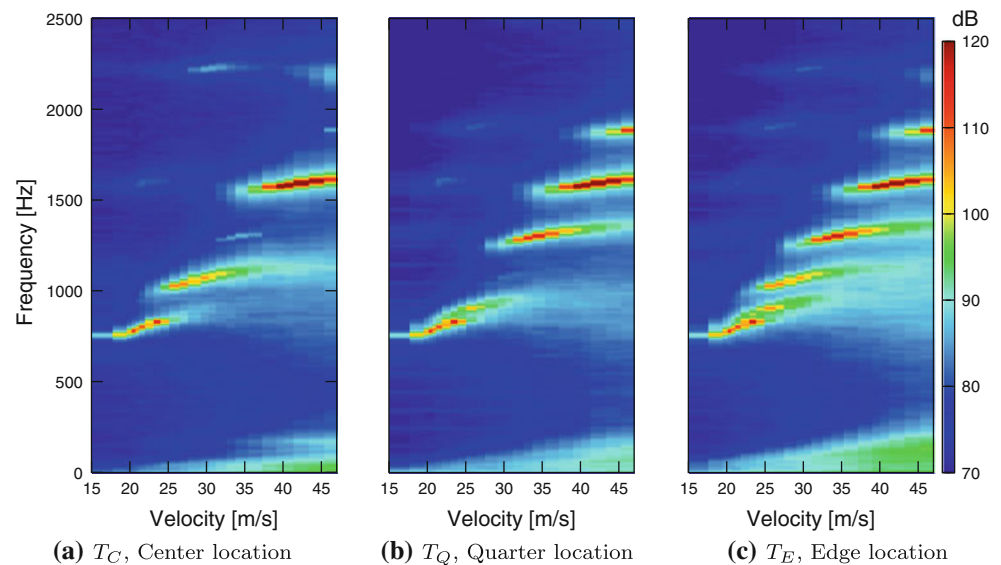
The flow velocity is increased incrementally. The internal sound pressure levels of these velocity sweeps are gathered in spectrograms and given in Fig. 6 for all 3 pressure transducer locations (locations as indicated in Fig. 2). The frequency of the excitation is shown at the vertical axis and the free stream velocity on the horizontal one. The pressure amplitude of the excitation is indicated in dB, with standard 2×10^{-5} Pa reference pressure. The figure shows several resonating modes with increasing velocity that have increasing mode frequencies. The first resonance mode is visible at all probe locations whereas for

Table 1 Boundary layer properties at 24 m/s

| Plate length (m) | δ^a | θ | H | δ_{99} | θ/L_o |
|------------------|------------|----------|------|---------------|--------------|
| 0.2 | 1.16 | 0.85 | 1.36 | 7.6 | 0.106 |
| 0.3 | 1.47 | 1.08 | 1.36 | 9.6 | 0.135 |
| 0.5 | 1.96 | 1.46 | 1.34 | 12.7 | 0.183 |
| 0.7 | 2.40 | 1.75 | 1.37 | 14.9 | 0.219 |
| 0.9 ^a | 2.81 | 2.05 | 1.36 | 17.3 | 0.256 |

Note that 0.9 m plate values are estimated using all other plate length data

^a Estimated

Fig. 6 Spectrograms of the three internal pressure probes, level by sound pressure (dB)

the higher modes some are not. This indicates a spanwise variation in the higher resonance modes.

From Fig. 6 it is found that all the center points of the excitation modes show a linear relation between frequency and velocity. The Strouhal number $Sr = \frac{fL_o}{U_\infty}$ corresponding to this is approximately 0.3, indicating that all modes are hydrodynamically excited by the first stage Rossiter mode (1967). No excitation of the second stage Rossiter mode ($Sr \approx 0.7$) is present, although low amplitude onsets of resonance for this Strouhal number can be observed in the upper left part of the figures by low amplitude horizontal excitation lines.

The observed higher modes frequencies are corresponding to the description in Sect. 2 (de Jong and Bijl 2010) regarding Eq. 2. The modes can be interpreted as separate sections acting as individual resonators that are coupled to each other or as a superposition of spanwise modes and the base Helmholtz resonance mode. The 6 observed modes correspond to the $n = 1$ –6 modes of Eq. 2. Modeled excitation frequencies are compared to the observed modes in Table 2. The spanwise wavelength of the equivalent spanwise mode λ_w is given in the table, together with the corresponding pressure node locations. The corrected vertical length of the cavity neck H'_o is set to match modeled and observed base mode frequency and is

then used to determine the expected higher mode frequencies. The predicted spanwise variations are in agreement with the observed pressure transducer nodes of Fig. 6. The $n = 2, 4, 6$ modes have a pressure node at the center transducer location, and the $n = 3$ mode has a node at the quarter location. For the first $n = 1$ mode around 800 Hz, the whole cavity is coherently excited and no nodes are present. The 3 pressure transducer signals are also in phase at this mode. Thus, for the base mode, acceptably uniform conditions across span are found.

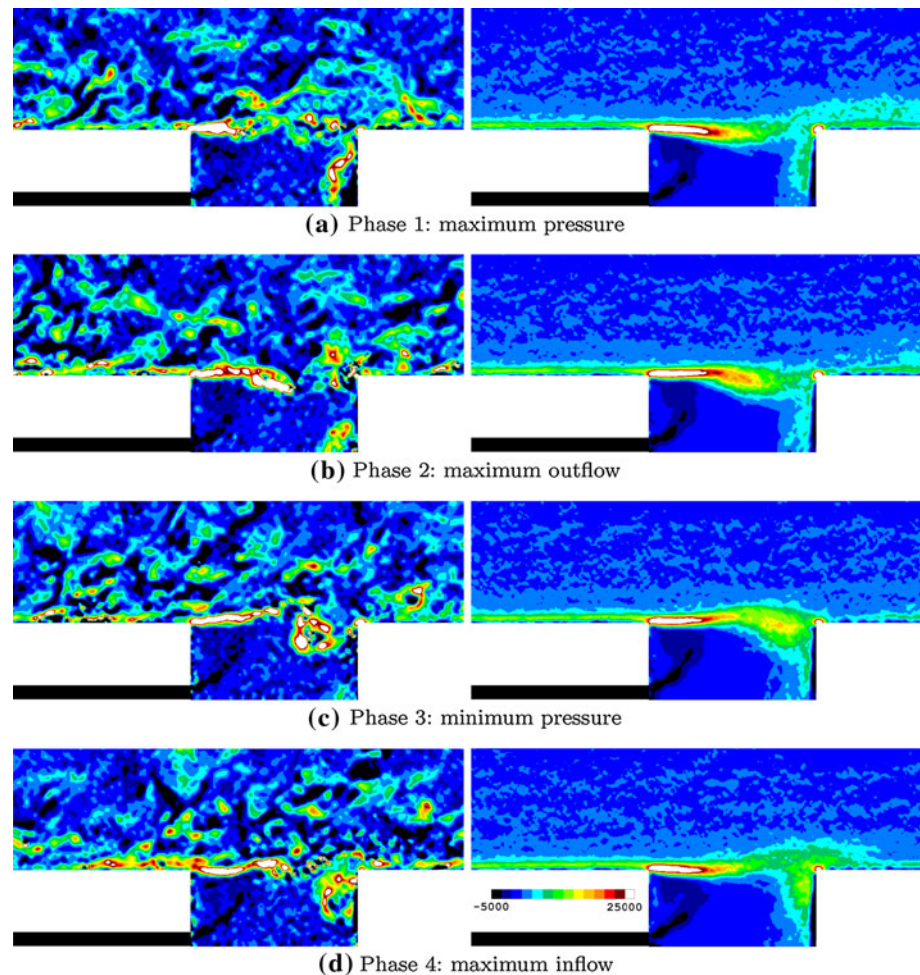
Even though the acoustic pressure amplitudes can be around 120 dB, it can be calculated that the energy transfer from flow to acoustics is low (Dequand et al. 2003). With the current cavity dimensions, Eq. 3 will give $\frac{|d\epsilon/dt|}{U_\infty} \approx 1 \times 10^{-2}$.

4.3 Shear layer characteristics

Both the time-resolved and phase-averaged PIV flow fields are given in Fig. 7 for four phases during a resonance cycle. The volume flow through the opening is used as a phase averaging indicating. The volume flow is calculated from the inflow velocity at $x/L_o = 0$ –1, $y/L_o = -0.5$. Using conservation of mass, the 4 chosen phases can be attributed with maximum cavity pressure,

Table 2 Comparison analytical model multiple Helmholtz resonators with flow run higher mode frequencies, $\beta = 0.97$

| Mode no. | Modeled freq. (Hz) | Observed freq. (Hz) | Spanwise wavelength λ_w | Location pressure nodes |
|----------|--------------------|---------------------|---------------------------------|------------------------------------|
| 1 | 830 (set) | 830 | n/a (Helmholtz) | n/a |
| 2 | 897 | 900 | $2/1W_o$ | $1/2W_o$ |
| 3 | 1,074 | 1,050 | $2/2W_o$ | $1/4W_o, 3/4W_o$ |
| 4 | 1,318 | 1,300 | $2/3W_o$ | $1/6W_o, 3/6W_o, 5/6W_o$ |
| 5 | 1,597 | 1,600 | $2/4W_o$ | $1/8W_o, 3/8W_o, 5/8W_o, \dots$ |
| 6 | 1,897 | 1,900 | $2/5W_o$ | $1/10W_o, 3/10W_o, 5/10W_o, \dots$ |

Fig. 7 Phase-averaged and instantaneous PIV results, negative spanwise vorticity $-\omega_z$ indicated, sharp upstream edge overhang, rounded downstream edge setup used. $-\omega_z$ range $-5,000$ to $25,000 \text{ s}^{-1}$ 

maximum outflow, minimum cavity pressure, and maximum inflow.

The time-resolved visualizations resolve the coherent fluctuations in the incoming boundary layer and their interactions with the separated shear layer on the cavity opening. The turbulent structures interact strongly with the cavity shear layer. It is believed that these turbulent structures influence the resonance behavior in two ways. First of all the structures directly perturb the cavity, enabling resonance onset. They also break up the shear layer, thereby reducing the resonance amplitude. Turbulent

structures can break up the spanwise coherency of the shear layer; however, this effect cannot be measured from the current PIV measurements at a single span. The shear layer shows both shear flapping motion (first half of the opening) and vortex roll up (second half of the opening). The shed vortices are partly transported into the cavity due to the interaction with the downstream edge.

In the phase-averaged representation, it is possible to identify more clearly the position of the shear layer corresponding to the 4 identified phases. Phase averaging distributes the vorticity so that a flapping shear layer with

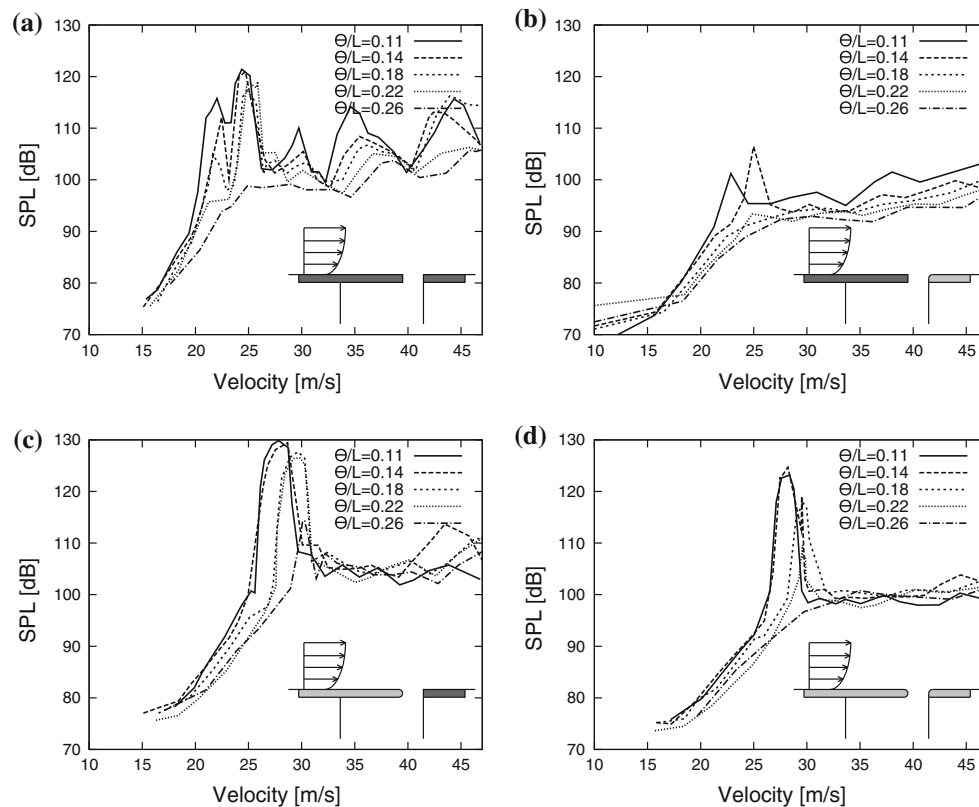


Fig. 8 Maximum cavity internal pressure excitation amplitude all upstream cover lip overhang configurations. The opening configuration is depicted in the graph

limited vortex roll-up appears in Fig. 7. The upstream part of the shear layer is stable and shows limited motion. Vortex roll-up occurs midway across the opening during the maximum outflow phase. This phase-averaged shear layer pattern is corresponding to the observations by Ma et al. (2009). The generated vortex is convected downstream and impinges on the downstream edge, where the vortex gets partly entrapped into the cavity. The influence of the interaction with turbulent fluctuations in the boundary layer manifests in a more diffuse shear layer compared to the instantaneous velocity fields.

5 Parametric analysis of resonance modes

5.1 Cavity acoustic response

Figure 8 shows the influence of the boundary layer thickness and opening geometry on the excitation results. In this figure, only the geometries with a cover lip attached at the upstream edge are considered. Figure 9 is a scaled representation of the amplitudes using Eq. 3, indicating the ratio of the acoustic velocity to the free stream velocity. One can observe that the acoustic amplitude in this case is relatively low, less than 1% of the mean flow in most cases.

With increasing boundary layer thickness, the resonance lock-on amplitudes diminish. Increasing the boundary layer thickness increases the stability of the shear layer, thereby reducing resonance (Michalke 1965, 1969, 1970). Some modes diminish with the $\theta/L_o = 0.22$ boundary layer and the $\theta/L_o = 0.26$ m boundary layer shows no resonance lock-on anymore for all modes.

The θ/L_o resonance threshold values found here are above ones observed in literature for shallow cavities of around $(\theta/L_o)_{\text{shallow}} \approx 1 \times 10^{-2}$ to 6×10^{-2} based on the current Reynolds number (Rockwell and Knisely 1979; Gharib and Roshko 1987; Sarohia 1977). This indicates an increased tendency to lock-on due to coupling with a resonator volume.

In literature described in Sect. 2 (Kooijman et al. 2008; Michalke 1965, 1969, 1970; Bruggeman et al. 1991), a limit stability Strouhal number of $St_{\theta, \text{max}} = 0.25$ was found based on stability properties of a tanh profile. This Strouhal number corresponds to a limiting boundary layer momentum thickness $\theta_{\text{max}} = 1.2$ mm and ratio over opening of $\frac{\theta}{L_o \text{max}} = 0.15$ above which no resonance is expected. According to Fig. 8, the stability limit is in the range $\frac{\theta}{L_o \text{max}} = 0.18$ – 0.26 , which is of the same order. The discrepancy can be attributed to the simplified tangent

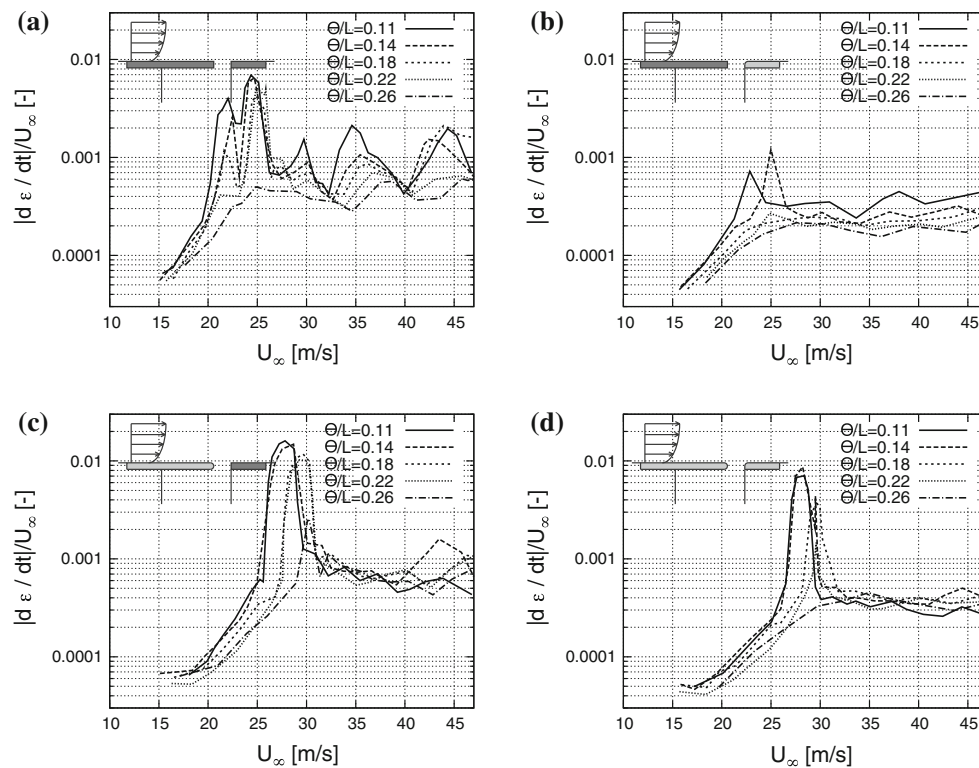


Fig. 9 Maximum cavity internal pressure excitation amplitude all upstream cover lip overhang configurations, amplitude scaled as relative acoustic velocity magnitude $\frac{|d\epsilon/dt|}{U_\infty}$.

hyperbolic profile that does not match the real shear layer profile. Further analysis of the shear layer stability is given in Sect. 5.2.

The shape of the upstream and downstream edges have different effects on the resonance amplitude. By comparing the upper and lower subfigures in Figs. 8 or 9, one can observe that rounding of the upstream edge will promote resonance. By comparing the left with the right subfigures, one can observe that rounding of the downstream edge will diminish resonance. The cause of the effects of the upstream and downstream edges will be analyzed separately in Sect. 5.3

Only cases with upstream sharp edge overhang show additional modes with spanwise variations appearing at higher velocities. There is currently no explanation why the higher modes only were excited for these configurations. One possible reason can be the modification of the acoustic diffraction due to the edges promoting the onset of higher modes, but this is not confirmed by the present investigation.

The onset velocity for base resonance is higher for cavity geometries with opening round-offs. Two reasons can be identified for this effect. The first possibility is a modification of the added resonating mass and thus a modification of the the resonance frequency according to Eq. 1. Secondly, the round-offs may modify the vortex

convection time over the opening, leading to a change in excitation frequency. Figure 10 shows the spectra at maximum base mode resonance for the 3 resonating geometries. The frequency at maximum base mode resonance is similar for all rounded and sharp edged geometries (840 ± 10 Hz), indicating that there is no significant change in added resonator mass. Therefore, the effect must be attributed to a modified excitation frequency due to the round-offs. Similar effects have been observed by Dequand et al. (2003). The change in excitation frequency can potentially be the result of a modified vortex path length

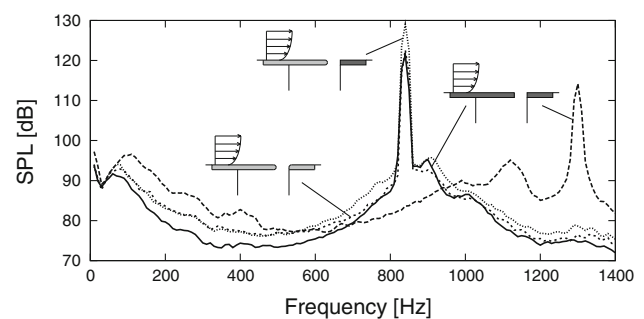


Fig. 10 Pressure spectra inside cavity at maximum base mode resonance, $\theta/L_o = 0.11$. For sharp edge geometry, one higher mode at 35 m/s is included in addition to the base mode spectrum

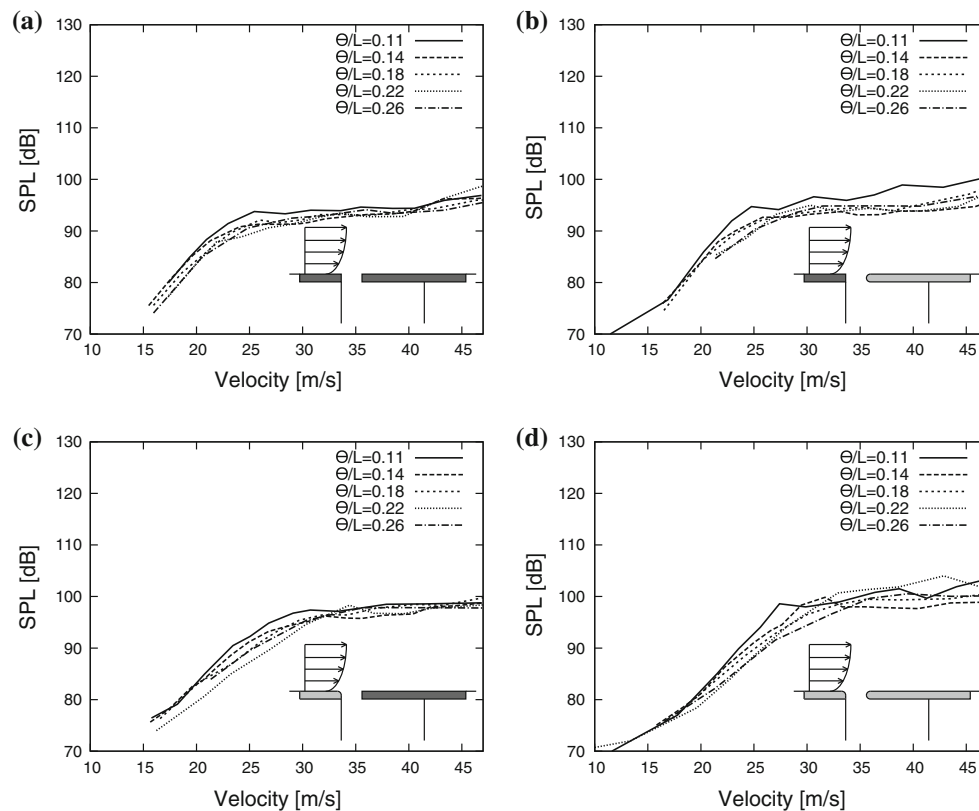


Fig. 11 Maximum cavity internal pressure excitation amplitude all downstream cover lip overhang configurations

due to the upstream and downstream round-offs and/or a modified vortex convection velocity over the opening.

Figure 11 shows the influence of the boundary layer thickness and opening geometry for the cases with a cover lip attached at the downstream edge. Figure 12 is a scaled representation of the amplitudes using Eq. 3, indicating the ratio of the acoustic velocity to the free stream velocity. When comparing Figs. 8 and 11, the most striking point is that only geometries with an upstream overhang produce resonance lock-on. The geometries with a downstream cover lip overhang show no resonance for all boundary layer thicknesses. This indicates that the resonance behavior of a resonator cannot be estimated without considering the details of the opening geometry and flow inside the cavity body. The large influence of the cover lip location on the resonance behavior will be further analyzed in Sect. 5.2

Scaled Fig. 12 reveals an influence of the cavity geometry on the non-resonant behavior. Non-resonant areas can be identified by sections where $|d\epsilon/dt|/U_\infty$ is independent of the velocity magnitude U_∞ . Table 3 gives the non-resonant average acoustic velocity $|d\epsilon/dt|/U_\infty$ for 30–45 m/s of the 4 largest boundary layer thicknesses ($L_p = 0.3, 0.5, 0.7, 0.9$ m). The table indicates that rounding of upstream as well as downstream edges

increases the passive response of the cavity. The effect of rounding the downstream edge in this non-resonant case differs from the influence during resonance, where rounding of the downstream edge diminishes resonance. This difference can be explained due to the fact that the non-resonant situation, acoustic energy losses (due to flow separation of the acoustic flow around the opening edges) are lower in case of a rounded downstream edge.

5.2 Physical effect of cover lip overhang

Time-averaged PIV results are used to explain the difference in response behavior between an upstream and downstream cover lip overhang. In the present research, we observed no resonance for the downstream overhang locations, even though they are acoustically identical to resonating upstream overhang geometries. When comparing the flow field in the cavity opening, an interesting difference can be observed. Figure 13 shows the mean flow patterns for an upstream and downstream cover lip overhang setup. Note that the geometries with sharp edges are used in this comparison.

A large steady recirculation in the opening is observed in case of a downstream overhang, causing a local cavity driven flow. The driven flow component is accounting for

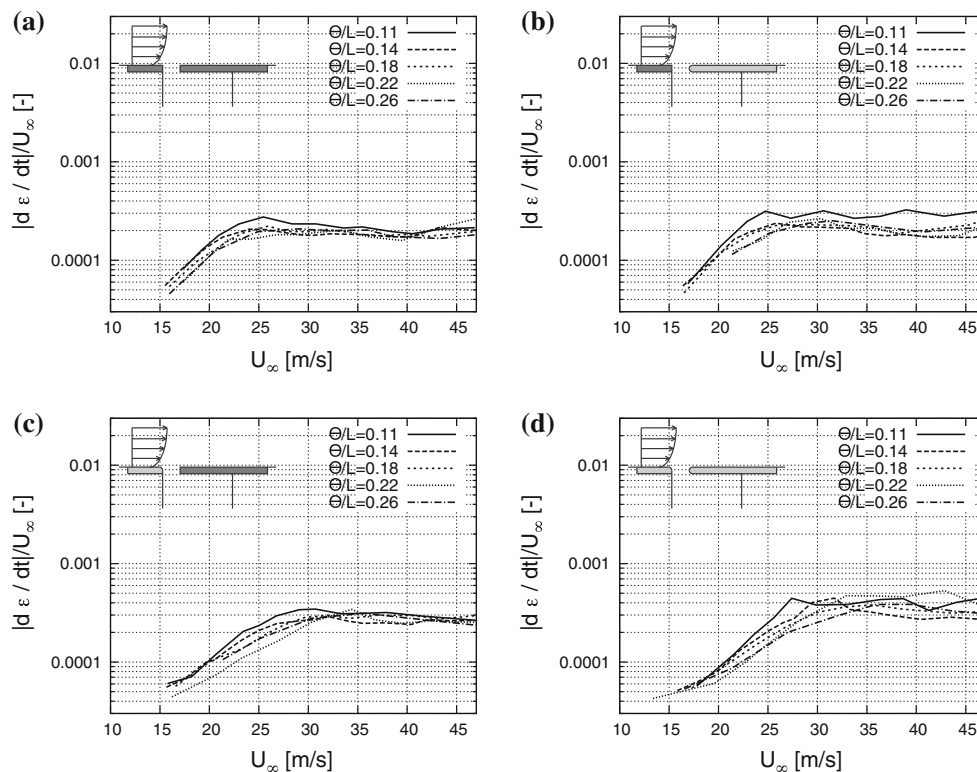


Fig. 12 Maximum cavity internal pressure excitation amplitude all mixed upstream cover lip overhang configurations, amplitude scaled as relative acoustic velocity magnitude $\frac{|d\epsilon/dt|}{U_\infty}$

Table 3 Non-resonant acoustic velocity amplitude response due to boundary layer fluctuations, downstream cover overhang

| | Downstream edge sharp | Downstream edge round |
|---------------------|-----------------------|-----------------------|
| Upstream edge sharp | 1.9×10^{-3} | 2.1×10^{-3} |
| Upstream edge round | 2.8×10^{-3} | 3.6×10^{-3} |

Average $|d\epsilon/dt|/U_\infty$, for velocity range of 30–45 m/s and 4 largest boundary layer thicknesses

an internal flow just below the opening of about $u_{int} \approx 0.1U_\infty$. In contrast, the upstream edge overhang shows an internal flow pattern with an inflow from the resonator volume and a separation region at the inner side of the upstream sidewall (visible in the lower left side of the Fig. 13a). This causes a considerably smaller cavity driven flow component compared to the downstream overhang geometry. The cavity driven flow influences the shear layer development along the opening. The effective shear is much lower for the downstream edge geometry and therefore the shear layer is more stable. This can be seen in the velocity plot of Fig. 14 and the effective shear given in Fig. 15. Here, one can clearly observe a reduction in shear between the geometries close to the upstream edge. This can greatly modify the stability behavior of the shear layer.

The vorticity thickness $\theta_\omega = \left(\frac{du}{dy}\right)_{max} / (U_\infty - u_{int})$ is not changed when scaled with respect to the effective velocity difference of the outer and inner cavity flow ($U_\infty - u_{int}$).

In order to quantify the difference between upstream and downstream overhang resonance behavior, linear stability analysis of Michalke (Kooijman et al. 2008; Michalke 1965, 1969, 1970; Bruggeman et al. 1991) is employed. To derive the properties of the current shear layer, profiles is beyond the scope of the current work and planned for a future investigation. However, the tangent hyperbolic profile can be used to provide an estimation for the inherent stability of the shear layer. As mentioned before in Sect. 2, Michalke found that a tanh profile is stable for Strouhal numbers $St_{\theta,max} = \frac{2\pi f \theta}{\Delta U} < 0.25$. Figure 16 shows the stream-wise velocity profiles midway across the opening for both the upstream and downstream overhang case. Included in the figure are fitted tanh profiles. The fitting parameters θ_{fit} , U_{fit}^-/U_∞ and U_{fit}^+/U_∞ are depicted in the figure. Using the fitting parameters and $U_\infty = 25$ m/s and $f_{res} = 840$ Hz will give $St_{\theta,fit} = 0.20 < St_{\theta,max}$ for the resonating upstream overhang case and $St_{\theta,fit} = 0.27 > St_{\theta,max}$ for the non-resonating downstream overhang case, confirming the difference in resonance behavior between the two cases. Note that there is a 35% difference between the upstream and downstream overhang Strouhal numbers. Also the

Fig. 13 Mean flow patterns in the cavity opening, color by normalized velocity magnitude $\frac{u}{U_\infty}$, with streamlines, sharp edges used

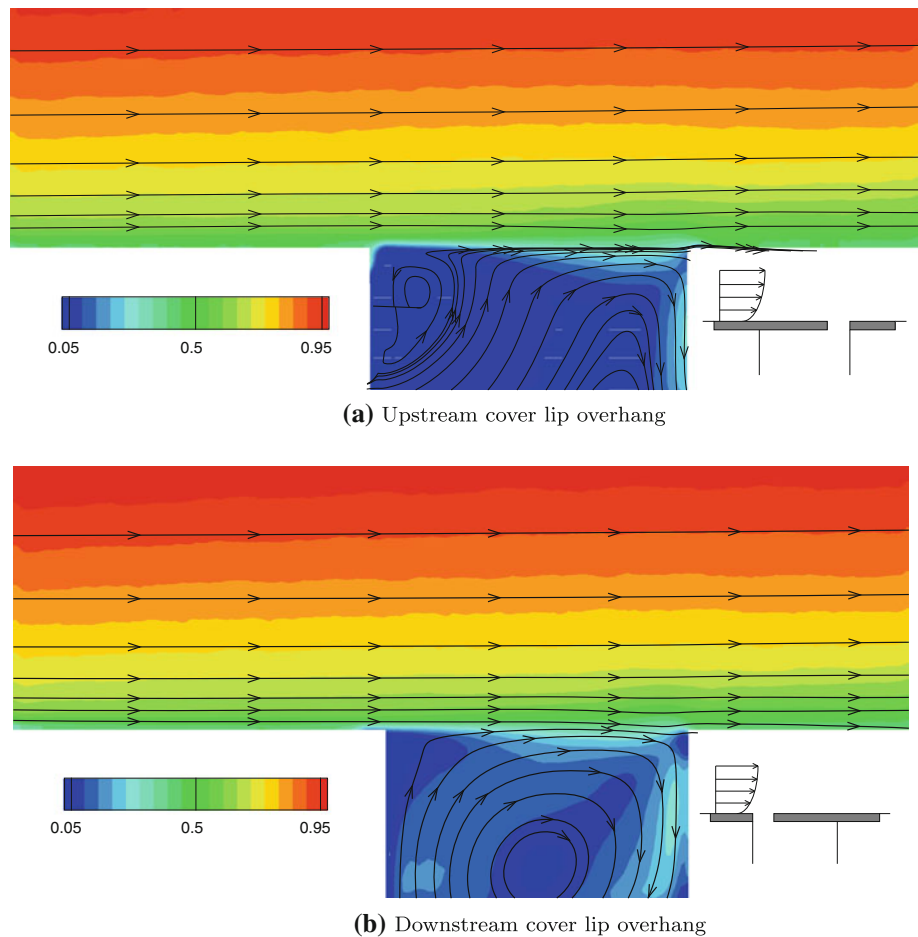
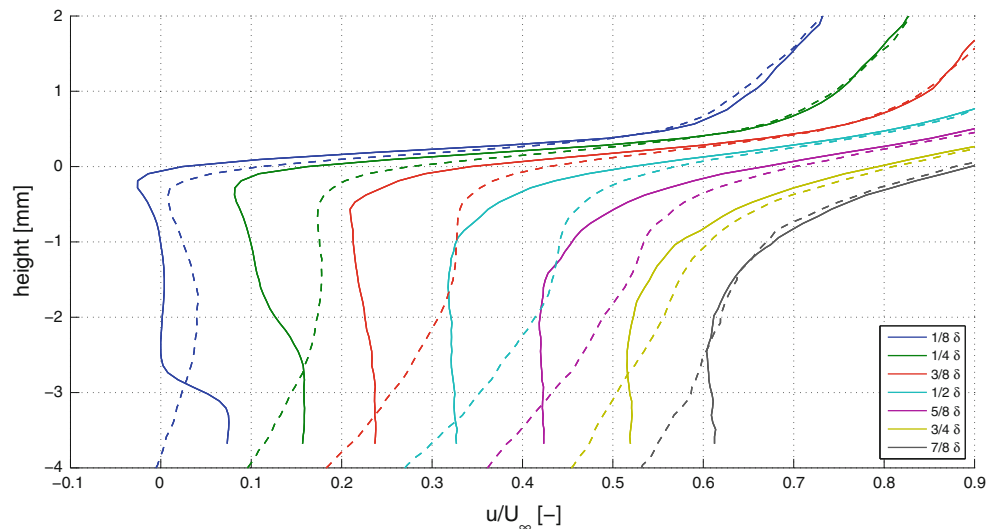


Fig. 14 Comparison of mean shear layer velocity profiles over the cavity opening. Plot in increments of $\Delta x = 1/8L_o$, starting at $x = 1/8L_o$. Lines separated by $0.1 \frac{u}{U_\infty}$ shifts. Solid lines show upstream lip overhang, dashed downstream lip overhang



difference in modeled cavity driven flow $\Delta U_{\text{fit}}^-/U_\infty = 0.12$ is expected to stabilize the downstream shear layer even further (Howe 1997, 1998). A more detailed analysis of the shear layer profiles is beyond the scope of the current work and planned for future investigations.

5.3 The role of edge rounding

As previously indicated, the resonance behavior is very sensitive to the edge geometry. Rounding of the downstream edge will reduce or even suppress the resonance

Fig. 15 Comparison normalized shear patterns $\frac{(du/dy)}{U_\infty/\theta_{bl}}$, over the cavity opening, with θ_{bl} the upstream boundary layer momentum thickness. Plot in increments of $\Delta x = 1/8 L_o$, starting at $x = 1/8 L_o$. Lines separated by $1.0 \frac{(du/dy)}{U_\infty/\theta_{bl}}$ shifts. Solid lines show upstream lip overhang, dashed downstream lip overhang

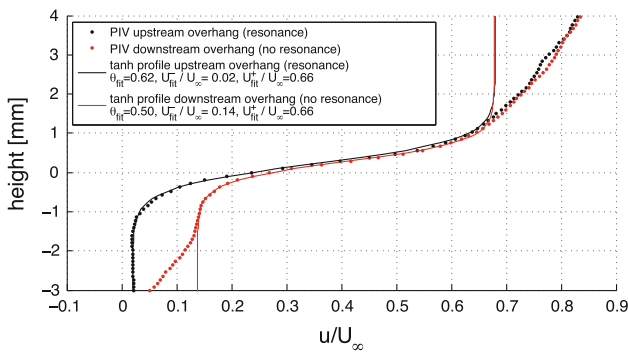
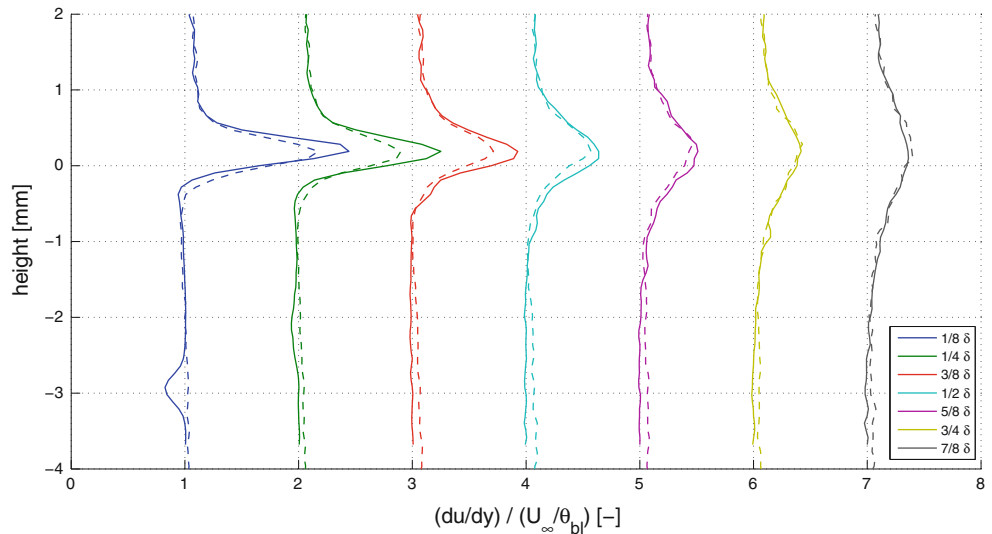
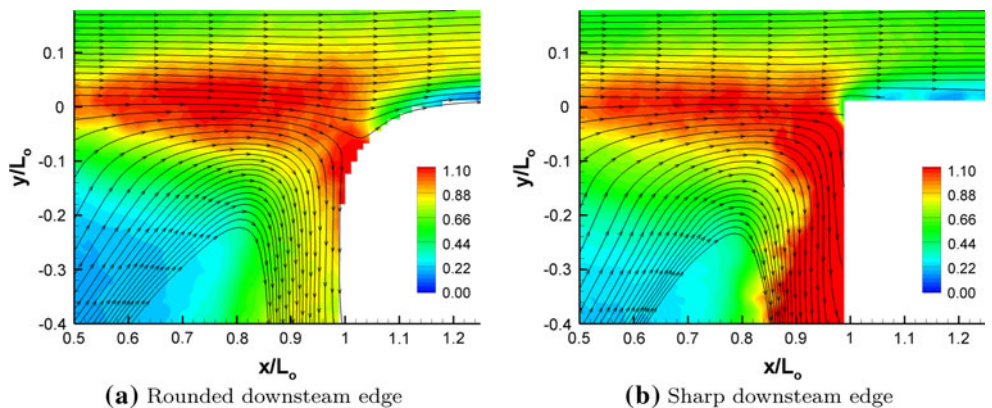


Fig. 16 Mean shear layer velocity profiles over the cavity opening at $x/L_o = 0.5$. Included are tanh profiles with fitted parameters

behavior. This has already been indicated in literature, where vortex-edge interaction plays a critical role (Kooijman et al. 2008; Rockwell and Knisely 1979). PIV results are used to aid the physical interpretation of the mechanism.

Figure 17 shows streamlines of the time-averaged flow field in the opening and scaled vertical velocity fluctuation

Fig. 17 Streamlines of mean flow with focus on the downstream edge, with scaled vertical velocity fluctuation magnitude in color $\frac{|v'|}{|v'|_p}$. The fluctuation magnitude is scaled using the fluctuation magnitude in the shear layer a point located midway across the opening ($x/L_o = 0.5, y/L_o = 0.0$)



magnitude $\frac{|v'|}{|v'|_p}$. The fluctuation magnitude is scaled using the fluctuation magnitude in the shear layer at a point $|v'|_p$ located midway across the opening ($x/L_o = 0.5, y/L_o = 0.0$). In this way, the fluctuation content can be compared independently of the amount of cavity feedback. The flow speed in this figure is 20 m/s and both cases have an upstream overhang lip with sharp upstream edges. Both cases do not have full resonance lock-on at these conditions.

The streamlines indicating a modified stagnation point location due to the downstream edge geometry. Also, the streamlines show a tendency of the flow to not get entrapped into the cavity, as the outside flow gets deflected outwards. This is confirmed by comparing $\frac{|v'|}{|v'|_p}$. Even though the shear layer fluctuation distribution is similar, more flow gets deflected into the cavity body.

By comparing the maximum lock-on amplitudes in Fig. 9, one can see that rounding of the upstream edge leads to an increase in resonance lock-on amplitude. Figure 18 shows the mean flow streamline patterns in the opening for the configurations with an upstream cover lip overhang. Left subfigures show rounded upstream edges,

Fig. 18 Streamlines of mean flow for all configurations with upstream cover lip overhang. Downstream mean flow stagnation point locations indicated by red bars

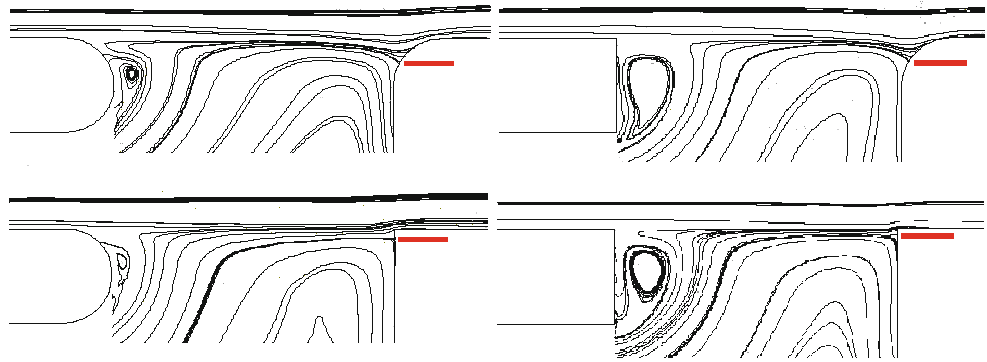
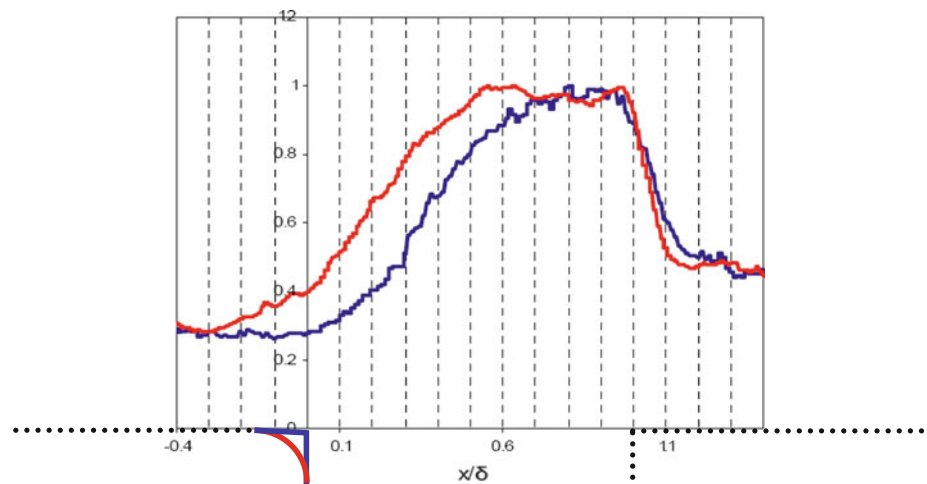


Fig. 19 y -velocity rms profiles in a streamwise rake over the shear layer, 0.5 mm above the opening, scaled with maximum observed y -velocity fluctuation $\frac{|v'|}{|v'|_{\max}}$. red rounded upstream edge, blue sharp upstream edge



right ones sharp upstream edges. Rounding of the upstream edge does not significantly change the mean flow pattern around the cavity opening.

An hypothesis for explaining the increased resonance amplitude in case of rounded upstream edges is that the free separation point of the rounded upstream edge compared to the fixed separation point of a sharp edge (due to Kutta condition) will decrease the stability of the shear layer. This is confirmed by examining vertical velocity fluctuation profiles scaled by maximum observed vertical velocity fluctuation $\frac{|v'|}{|v'|_{\max}}$ of the shear layer in Fig. 19. The shear layer show larger fluctuations in the first section, even upstream of the rounded edge. Also the effective streamwise opening length is larger for the rounded edge, which promotes larger deflections at the downstream edge. In turn, this effect may cause a large amount of turbulent fluctuations to be entrained inside of the cavity.

6 Conclusions

An experimental investigation has been performed on simplified slender cavities that resemble automotive doors.

A parametric study on the influence of the cavity opening geometry and boundary layer properties is conducted.

Several configurations showed resonance lock-on, where the acoustic velocity is about 1% of the free stream velocity. Higher modes with spanwise variations are observed, but only for some investigated geometries. The modes are described by a simple analytical model of coupled Helmholtz resonance with spanwise room modes.

The shear layer shows both flapping shear layer and vortex roll-up behavior. The shear layer growth is dominated by interaction with the turbulent boundary layer. Resonance behavior is highly sensitive to the boundary layer thickness. There is a cutoff boundary layer thickness compared to the opening length above which no resonance occurs.

Only geometries with an upstream cover lip overhang show resonance lock-on behavior. The difference in lock-on behavior between upstream and downstream edge overhangs can be explained by driven cavity internal flow patterns.

Rounding of the downstream edge reduces lock-on amplitude due to a reduction in flow entrapment into the cavity, thereby lowering feedback. Rounding of the

upstream edge promotes resonance due to the increased mobility and instability of the shear layer, and an increased streamwise length to grow large deflections.

Acknowledgements We would like to thank Mico Hirschberg for his helpful advice. We also would like to thank Stefan Bernardy and Sina Ghaemi for help with the experimental setup.

Open Access This article is distributed under the terms of the Creative Commons Attribution Noncommercial License which permits any noncommercial use, distribution, and reproduction in any medium, provided the original author(s) and source are credited.

References

- Ahuja K, Mendoza J (1995) Effects of cavity dimensions, boundary layer, and temperature on cavity noise with emphasis on benchmark data to validate computational aeroacoustic codes. NASA/CP, pp 1–284
- Bruggeman J, Hirschberg A, Dongen MV, Wijnands A, Gorter J (1991) Self-sustained aero-acoustic pulsations in gas transport systems: experimental study of the influence of closed side branches. *J Sound Vib* 150:371–393
- Coltman JW (1976) Jet drive mechanism in edge tones and organ pipes. *J Acoust Soc Am* 60:725–733
- Crouse B, Senthoooran S, Balasubramanian G, Freed D, Noelting S, Mongeau L, Hong JS (2005) Sunroof buffeting of a simplified car model: simulations of the acoustic and flow-induced responses. SAE 2005-01-2498, pp 2498–2513
- de Jong AT, Bijl H (2010) Investigation of higher spanwise helmholtz resonance modes in slender covered cavities. *J Acoust Soc Am* 128:1668–1678
- Dequand S, Hulshoff SJ, Hirschberg A (2003) Self-sustained oscillations in a closed side branch system. *J Sound Vib* 265:359–386
- Dequand S, Luo X, Willems J, Hirschberg A (2003) Helmholtz-like resonator self-sustained oscillations, part 1: acoustical measurements and analytical models. *AIAA* 41:408–415
- Dequand S, Hulshoff S, Kuijk van H, Willems J, Hirschberg A (2003) Helmholtz-like resonator self-sustained oscillations, part 2: detailed flow measurements and numerical simulations. *AIAA* 41:416–424
- Dequand S, Willems JFH, Leroux M, Vullings R, van Weert M, Thieulot C, Hirschberg A (2003) Simplified models of flue instruments: influence of mouth geometry on the sound source. *J Acoust Soc Am* 113:1724–1735
- Elder SA (1973) On the mechanism of sound production in organ pipes. *J Acoust Soc Am* 54:1554–1564
- Elder SA, Farabee TM, DeMetz FC (1982) Mechanisms of flow-excited cavity tones at low mach number. *J Acoust Soc Am* 72:532–549
- Gharib M, Roshko A (1987) The effect of flow oscillations on cavity drag. *J Fluid Mech* 177:501–530
- Gloerfelt X (2009) Cavity noise. http://sin-web.paris.ensam.fr/squelettes/ref_biblio/Gloerfelt_VKI_2009a.pdf (date last viewed 10/26/09)
- Haigermoser C, Scarano F, Onorato M (2009) Investigation of the flow in a circular cavity using stereo and tomographic particle image velocimetry. *Exp Fluids* 46:517–526
- Henderson BS (2000) Category 6 automobile noise involving feedback—sound generated by low speed cavity tones. NASA Tech. Rep., pp 95–100
- Henderson BS (2004) Category 5: sound generation in viscous problems, problem 2: sound generation by flow over a cavity. NASA Tech Rep, pp 71–77
- Howe MS (1997) Low strouhal number instabilities of flow over apertures and wall cavities. *J Acoust Soc Am* 102:772–780
- Howe MS (1997) Influence of wall thickness on rayleigh conductivity and flow-induced aperture tones. *J Fluids Struct.* <http://linkinghub.elsevier.com/retrieve/pii/S088997469790087>
- Howe MS (1998) Rayleigh conductivity and self-sustained oscillations. *Theor Comput Fluid Dyna.* <http://www.springerlink.com/index/KDM7PK8CT648E5W8.pd>
- Ingard U (1953) On the theory and design of acoustic resonators. *J Acoust Soc Am* 25:1037–1061
- Kooijman G, Hirschberg A, Golliard J (2008) Acoustical response of orifices under grazing flow: effect of boundary layer profile and geometry. *J Sound Vib* 315:849–874
- Ma R, Slaboch P, Morris S (2009) Fluid mechanics of the flow-excited helmholtz resonator. *J Fluid Mech* 623:1–26
- Michalke A (1965) On spatially growing disturbances in an inviscid shear layer. *J Fluid Mech* 23:521–544
- Michalke A (1969) The influence of the vorticity distribution on the inviscid instability of a free shear layer. *Fluid Dyna Trans* 4:751–770
- Michalke A (1970) The instability of free shear layers, a survey on the state of art. *Deutsche Luft- und Raumfahrt Mittlung*, p 70
- Mongeau L, Bezemek JD, Danforth R (1997) Pressure fluctuations in a flow-excited door gap model. SAE, pp 1–7, sAE-971923
- Morris S (2011) Shear layer instabilities: particle image velocimetry measurements and implications for acoustics. *Annu Rev Fluid Mech* 43:3692. <http://www.annualreviews.org/doi/abs/10.1146/annurev-fluid-122109-160742>
- Nelson PA, Halliwell NA, Doak PE (1981) Fluid dynamics of a flow excited resonance, part I: experiment. *J Sound Vib* 78:15–38
- Nelson PA, Halliwell NA, Doak PE (1983) Fluid dynamics of a flow excited resonance, part II: flow acoustic interaction. *J Sound Vib* 91:375–402
- Radavich PM, Selamet A, Novak JM (2001) A computational approach for flow-acoustic coupling in closed side branches. *J Acoust Soc Am* 109:1343–1353
- Ricot D, Maillard V, Bailly C (2001) Numerical simulation of the unsteady flow past a cavity and application to sunroof buffeting. In: 7th AIAA/CEAS aeroacoustics conference, pp 1–11. Maastricht, The Netherlands. aIAA 2001–2112
- Rockwell D, Knisely C (1979) The organized nature of flow impingement upon a corner. *J Fluid Mech* 93:413–432
- Rockwell D, Naudascher E (1979) Self-sustained oscillations of impinging free shear layers. *Annu Rev Fluid Mech* 11:67–94
- Rossiter JE (1967) Wind-tunnel experiments on the flow over rectangular cavities at subsonic and transonic speeds, 1st edn. H.M.S.O., London, pp 1–32
- Sarohia V (1977) Experimental investigation of oscillations in flows over shallow cavities. *AIAA J* 15:984–998
- White FM (1991) Viscous fluid flow, 2nd edn. McGraw-Hill, New York, pp 409–413